2023 IEEE/ASME International Conference on Advanced Intelligent Mechatronics (AIM)
June 28-30, 2023. Seattle, Washington, USA

Design and Analysis of a Compliant Mechanism with Variable Stiffness

Weipeng Zhang[1], and Peng Yan[1], *SeniorMember,IEEE*

***Abstract*— This paper presents the design and analysis of a variable stiffness flexure mechanism with a novel normal-stress electromagnetic stiffness tunable actuator (NESTA). Aiming at real-time stiffness adjustment of flexible mechanisms, the proposed method employs a combination of flexible guiding assembly and the NESTA structure. The static model of the proposed mechanism is developed, including the analysis of the static electromagnetic force and the electromagnetic stiffness, as well as the stiffness of the flexible guide assembly. The electromagnetic stiffness adjustment capability is further evaluated by finite element software COMSOL. The effect of mechanism stiffness adjustment on mechanism characteristics is also analyzed by multi-physics field coupled finite element simulation, which demonstrates the nonlinear characteristics associated with the armature position.**

I. INTRODUCTION

With the development of micro/nanotechnology, flexible mechanism is extensively applied to advanced manufacturing or ultra-high precision motion system. Flexible mechanism were required by high-aspect-ratio micro-fabrication, such as high energy beam processing [1], reactive ion etching [2], and nanoimprinting [3], as well as large-strokes and high-precision operations, such as atomic force microscopes [4], semi- conductor lithography [5], and fast tool servo-assisted machining instruments [6]. The ultra-high precision motion is usually achieved through the elastic deformation of compliant mechanisms [7], [8], However, once the flexible mechanisms are designed and manufactured, its stiffness generally cannot be adjusted, which leads to an unavoidable trade-off between motion travel and mechanical bandwidth. The variable stiffness mechanism with a flexible mechanism can significantly improve the precision, carrying and anti-disturbance capability of precision systems. This expands the range of applications in human-computer interaction and other applications.

The variable stiffness machine is referred to an adaptive flexible system in which the stiffness can be reconfigured and controlled. Variable stiffness actuators (VSAs) are used to adjust the stiffness to improve compliance and versatility. For example, higher-stiffness configurations enable faster response and better fidelity performance, while lower-stiffness configurations reduce the impact of collision and achieve safer and more stable force and torque output[9],[10]. VSAs are categorized into three general groups based on how they vary their stiffness, including adjusting the spring preload[11], changing the transfer ratio of the load force[12], and changing the physical characteristics of the spring[13]. While each of these categories has specific advantages, they suffer from the common limitations: the need for additional components and mechanisms which leads to increased complexity, weight, size, and assembly time, difficulty in building models, and the introduction of additional inertial forces. However, to realize variable stiffness mechanisms, some articles suggested that the configuration of stiffness can be achieved by using piezoelectric actuators with flexible leaf springs through the stress-toughening effect of the leaf springs[14].There is a investigation to obtain negative stiffness mechanisms by means of lateral nonlinear springs generating a squeezing force on the intermediate load, which is converted into a force in the direction of motion away from the load balance position [15],[16]. Since the deformations of the leaf springs cannot be precisely controlled, the realization of variable stiffness with flexible mechanisms remains a challenge.

Note that the normal-stress electromagnetic actuator (NSEA) is widely used in the field of micro and nano for its fast response, non-contact, compact structure and easy control[17]. The nonlinearity of NESA is useful to provide electromagnetic negative stiffness[18],19]. Compared to mechanical variable negative stiffness, electromagnetic variable negative stiffness has the characteristics of non-friction, non-mechanical fatigue and non-contact[20], so it can effectively avoid redundancy of the mechanism and provide convenient real-time online stiffness adjustment. Therefore, it is necessary to develop a novel variable stiffness mechanism that can provide real-time online stiffness adjustment by adopting the tunable stiffness of NESA combined with a flexible mechanism.

In this paper, we propose a novel variable stiffness mechanism, inventively apply a negative stiffness adjustment structure based on the principle of normal stress electromagnetic actuation to flexible mechanism. In addition, we developed a static model of the variable stiffness mechanism, including the derivation of the negative electromagnetic stiffness under magnetic static and the positive stiffness model of the flexible mechanism. Meanwhile, the finite element simulations are performed to verify the adjustable negative electromagnetic stiffness of the designed electromagnetic variable stiffness actuator and the mechanics performance of the flexible mechanism. Finally, the tunable stiffness characteristics of the variable stiffness mechanism are analyzed by coupled multi-physics simulation

[1]Peng Yan is with Key Laboratory of High-efficiency and Clean Mechanical Manufacture, Ministry of Education, School of Mechanical Engineering, Shandong University, Jinan, Shandong, 250061, China yanpeng@sdu.edu.cn

[1]Weipeng Zhang is with Key Laboratory of High-efficiency and Clean Mechanical Manufacture, Ministry of Education, School of Mechanical Engineering, Shandong University, Jinan, Shandong, 250061, China

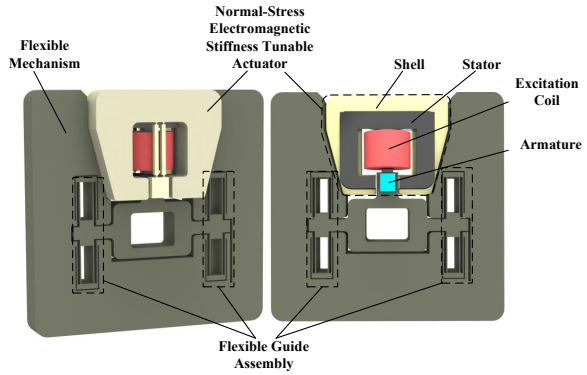

Fig. 1. Structure of the variable stiffness mechanism

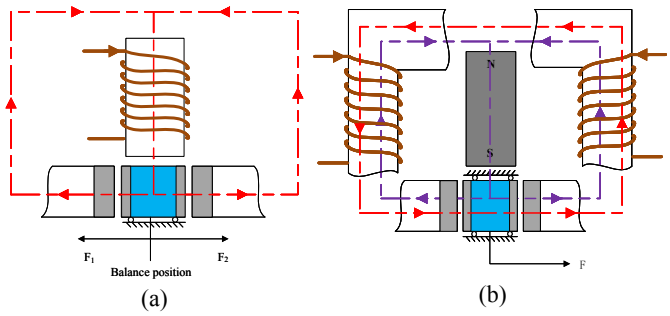

Fig. 3. Principle of the NESTA (a) design of electromagnetically variable negative stiffness (b) conventional NESA of directly driven.

II. CONFIGURATION AND PRINCIPLE

The NSEA is commonly used in previous research to produce kinetic energy to drive flexible mechanisms so that it can be used as a energy generator. However, the generated electromagnetic potential energy which usually shows a negative stiffness characteristic is controlled by the driving current. According to the above principle, the structure of the variable stiffness mechanism was designed in this paper as shown in Fig. 1. In order to avoid initial electromagnetic forces, the flux of the NESTA should be symmetrically positioned, so that the excitation coil is arranged on the middle stator. The armature is arranged in the middle balance position while being attached to the swing link guide. At the same time, the NESTA is simultaneously connected in parallel with the end output position of the flexible mechanism. In one word, the whole mechanism is composed of an electromagnetic negative stiffness unit and a positive stiffness flexible unit, the stiffness of the mechanism will be adjusted by the excitation current of the NESTA.

A. Normal-stress electromagnetic stiffness tunable actuator

The assembly of electromagnetic variable negative stiffness for NESTA is schematically illustrated in Fig. 2. This NESTA is composed of a mover, the stators, the excitation coil and shells. The stators is consists of T-shaped stator and L-shaped stator, which are positioned in shells. Both the stators and the mover are manufactured by Permalloy, which is a soft magnetic material with high permeability to provide a low resistance path for the magnetic flux. The excitation coil is tightly wound by enameled wire and arranged on the middle column of the T-stator. The mover(also called the armature) is installed in a frame extending from the main system's stage where it serves as a pivot for transferring negative stiffness. The shells are separated into the upper and lower parts. Except to fix the stator, the shells can locate the relative position of the movers through the angles on the sides.

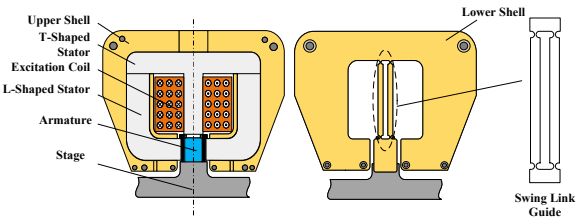

Fig. 2. The assembly of electromagnetic variable negative stiffness for the NESTA.

As shown in Fig. 3(a), when the coil is excited, the magnetic flux will be limited in the circuits consisting of the stator and the movers. When the mover is located in the middle balance position, the flux density in the air gap at both sides of the mover is almost the equivalent, so that the resultant force to the mover is zero. When the main stage moves to the left, the mover will be closer to the left stator pole, with the left air gap flux density increasing. At the same time, the right air gap flux density decreases. Thus the direction of the resultant force loaded on the mover is left, the electromagnetic force will be contributed to move the mover away from the balance position. It is similarly when the main motion stage moves to the right. As it is seen, the magnetic circuit configuration is capable of generating negative electromagnetic stiffness applied to the movers. As shown in Fig. 3(b), where NESAs are used as the main actuators, permanent magnet is usually arranged in the middle to reduce the nonlinear output of the actuators. Different from this design, the NESA in this study obtain the ability of variable stiffness through symmetrical arrangement of the yoke without permanent magnets.

B. Structure of parallel connection between electromagnetic and flexible mechanical

In this study, a parallel connection of the electromagnetic negative stiffness with the positive stiffness mechanism is used for better stiffness adjustment performance of the variable stiffness mechanism. The relative mounting positions of the NESTA and the flexible mechanism are shown in Fig. 4. Note that as the negative electromagnetic stiffness increases, the instability of the system also grows. To improve this weakness, the compound parallel guide mechanism (CPGM) is applied here as a flexible mechanism. At the same time, this mechanism is able to minimize the influence of the guide mechanism stiffness and obtain excellent guiding performance

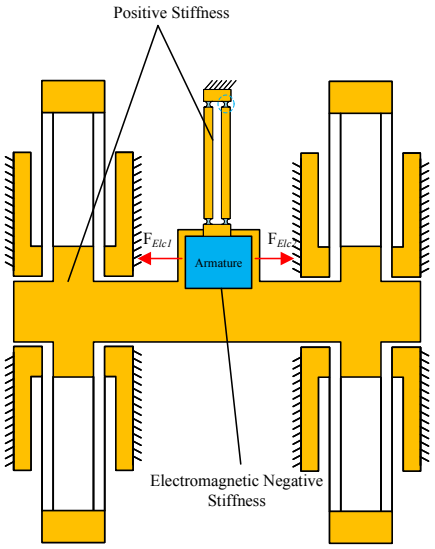

Fig. 4. Structure of parallel connection between electromagnetic and flexible mechanism

III. MODELING OF VARIABLE STIFFNESS MECHANISM

Stiffness is used to describe the degree of an object deforms under force, this principle is applied to electromagnetism drive, the electromagnetic stiffness is defined to the derivative of the electromagnetic force F with displacement x as:

$$k_e = \frac{dF}{dx}, \tag{1}$$

where k_e is the stiffness of the NESTA. The normal stress actuation has a high force density, so it means that this form of electromagnetic actuator is able to produce a higher electromagnetic stiffness compared to other types of electromagnetic actuators. The net actuating force of The NESTA is due to the difference in the attraction of the left and right magnetic poles to the armature. The resultant force acting on the armature is:

$$F = F_R - F_L. \tag{2}$$

In this paper, Maxwell stress tensor theory is used to calculate the net actuating force on the armature. While the DC flux generation is investigated, the total fluxes generated by the excitation coil windings. As shown in Fig. 5, the flux is divided into two perfectly symmetrical closed circuit on the left and right. The left and right coil windings generate flux densities B_L and B_R respectively. The electromagnetic forces acting on the left and right pole areas of the armature are calculated by applying the Maxwell stress tensor theory:

$$F_L = \frac{B_L^2 S_{arm}}{2\mu_0}, F_R = \frac{B_R^2 S_{arm}}{2\mu_0}, \tag{3}$$

where μ_0 is the vacuum permeability, S_{arm} is the armature pole face area. After the magnetic circuit is stabilized, it is illustrated that the magnetic circuit is not saturated, so the permeability in the core does not change and the B-H curve in the stator core is in a linear position. Then, the magnetic circuit can be divided into several uniform segments. Applying Gauss's Law to the armature (ignore assembly gaps and magnetic leakage), the following is derived:

$$B_L S_{\text{arm}} + B_R S_{\text{arm}} = NIS_{\text{arm}}, \tag{4}$$

where NI is the number of Ampere-turns of the total coil windings, μ_r is the relative magnetic permeability inside the stator core of soft magnetic material. To the left and right side closed loop magnetic circuit, applying Ampere's Loop Laws and the following is obtained:

$$\frac{B_L}{\mu_0}\left(g+\Delta x+\frac{L_{sta}}{2\mu_r}+\frac{L_{arm}}{2\mu_r}\right)=\frac{NI}{2}, \tag{5}$$

Similarly, to the right closed loop magnetic circuit, applying Ampere's Loop Laws and the following is obtained:

$$\frac{B_R}{\mu_0}\left(g-\Delta x+\frac{L_{sta}}{2\mu_r}+\frac{L_{arm}}{2\mu_r}\right)=\frac{NI}{2}, \tag{6}$$

Setting $L = L_{sta} + L_{arm}$ and simplifying Eq.(5) and Eq.(6), the DC fluxes in both air gaps can be expressed as:

$$\begin{cases} B_L = \frac{\mu_0\mu_r NI}{2\mu_r(g+\Delta x)+L} \\ B_R = \frac{\mu_0\mu_r NI}{2\mu_r(g-\Delta x)+L}. \end{cases} \tag{7}$$

substituting Eq.(7) into Eq.(3) and Eq.(2) leads to:

$$\begin{aligned} F &= F_R - F_L \\ &= \frac{N^2I^2\mu_r{}^2\mu_0 S_{\text{arm}}}{2}\left[\frac{1}{(2\mu_r(g-\Delta x)+L)^2}-\frac{1}{(2\mu_r(g+\Delta x)+L)^2}\right], \end{aligned} \tag{8}$$

substituting Eq.(8) into Eq.(1) leads to

$$\begin{aligned} k_e &= \frac{dF}{dx} \\ &= 2N^2I^2\mu_r{}^3\mu_0 S_{\text{arm}}\left[\frac{1}{(2\mu_r(g-\Delta x)+L)^3}+\frac{1}{(2\mu_r(g-\Delta x)+L)^3}\right] \\ &= 2N^2I^2S_{\text{arm}}\mu_0\left[\frac{1}{\left(2(g-\Delta x)+\frac{L}{\mu_r}\right)^3}+\frac{1}{\left(2(g-\Delta x)+\frac{L}{\mu_r}\right)^3}\right]. \end{aligned} \tag{9}$$

In Eq.(8), To facilitate analysis, the magnetoresistance in the stator core is ignored as $\mu_r \sim \infty$, So the stiffness of the NESTA in the equilibrium position can be expressed as:

$$\lim_{\Delta x\to 0} k_e = \frac{N^2I^2S_{\text{arm}}\mu_0}{2g^3}. \tag{10}$$

From Eq. (10), it can be concluded that the negative stiffness produced by NESTA will be determined by the NI of the excitation coil, when all the solid parameters are determined. Furthermore, it doesn't change the value of the electromagnetic negative stiffness by changing the direction of the current.

Further, the positive stiffness flexible mechanism is modeled. Firstly, the local coordinate system of the the circular notched hinge is shown in Fig. 6(a). According to the flexibility matrix method[21], the matrix of the swing link guide $\mathbf{C}^{SG}$ is as:

$$\mathbf{C}^{SG} = \mathbf{C}^{ci} + \mathbf{A}^{\mathrm{T}}\mathbf{C}^{pr}\mathbf{A} + \mathbf{B}^{\mathrm{T}}\mathbf{C}^{ci}\mathbf{B}, \tag{11}$$

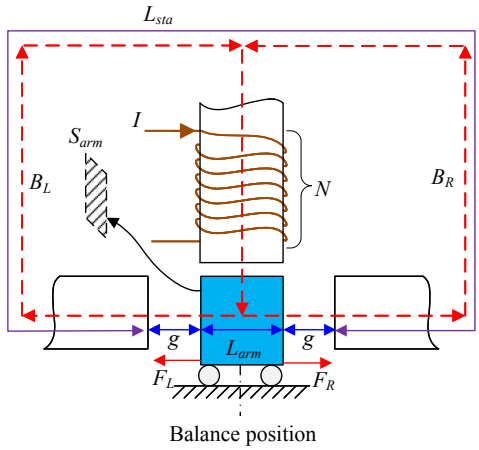

Fig. 5. the excitation coil circuit of the NESTA and equivalent model

where $\mathbf{A}$, $\mathbf{B}$ is the transformation matrix , which are as follows:

$$\mathbf{A}=\begin{bmatrix}1&0&0\\0&1&l_1\\0&0&1\end{bmatrix},\mathbf{B}=\begin{bmatrix}1&0&0\\0&1&l_1+2r_{ci}\\0&0&1\end{bmatrix}, \quad (12)$$

where $\mathbf{C}^j$ is the compliance factor in different directions, $j=ci$ or pr, ci means circular notched hinge and pr means prismatic hinge, the specific values are as mentioned in the literature [21].

Combining the above Eq. (11), the stiffness of the swing link guide k_{GFO} is as follows:

$$k_{GFO}=\frac{1}{\mathbf{C}_{22}^{SG}}, \quad (13)$$

where $\mathbf{C}_{22}^{SG}$ is the flexibility matrix coefficient. Similarly , the stiffness of a single beam is calculated as

$$k'=\frac{1}{\mathbf{C}_{22}^{pr}}, \quad (14)$$

from the parallel relationship, the stiffness of CPMG k_{CPGM} can be obtained as:

$$k_{CPGM}=16k'. \quad (15)$$

In summary, the total stiffness of the variable stiffness mechanism K is expressed according to the stiffness parallelism relationship as

$$K=k_{GFO}+k_{CPGM}-k_e. \quad (16)$$

IV. ANALYSIS OF VARIABLE STIFFNESS MECHANISM

In order to more accurately analyze the electromagnetic force, the electromagnetic negative stiffness characteristics and the stiffness tunability of the proposed variable stiffness mechanism, both the electromagnetic and mechanical properties of the variable stiffness mechanism are simulated through the software named COMSOL Multiphysics. whose parameters are set as those presented in sections.

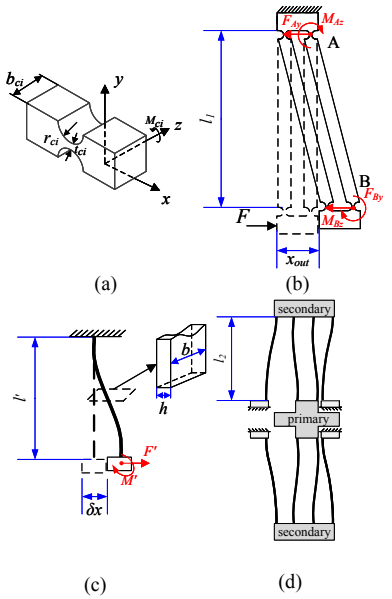

Fig. 6. Model of flexible mechanism (a) circular notched hinge(b) the swing link guide (c) deformation of individual flexure beam (d)the compound parallel guide mechanism

A. Parameters of the variable stiffness mechanism

Combined with the above system static modeling, the influential parameters affecting the electromagnetic variable stiffness actuator include: number of coil turns N, coil current I, air gap g, assembly clearance L_{ac}, and pole size S_{arm}. The assembly and shape configuration should reduce the magnetic leakage of the electromagnetic stiffener and thus reduce the energy loss of the electromagnetic stiffener. Therefore, the electromagnetic stiffening mechanism is configured with an aluminum alloy housing with small magnetic permeability, and the assembly gap is minimized. From the static analysis of the electromagnetic stiffening mechanism, it can be seen that the smaller the air gap, the greater the negative stiffness. Therefore, reducing the air gap to meet the stroke is an effective measure to improve the output

TABLE I
PARAMETERS OF FEA

Parameters	*Symbol*	*Value*	*Unit*
Length of working air gap	g	2	mm
Length of stator	$Lsta$	197	mm
Length of armature	$Larm$	12	mm
Length of the assembly clearance	Lac	1.5	mm
Length of the swing link guide	l_1	43	mm
Length of CPGM's individual flexure beam	l_2	26	mm
Thickness	b	25	mm
Young's modulus	E	72.1	GPa
Poisson's ratio	μ	0.45	/
Hinge thickness	h	0.5	mm
Density	σ	2.73×10^3	kg/m^3

efficiency of negative stiffness.

In addition to the influence of the assembly configuration on the electromagnetic stiffening actuator, the number of turns of the coil and the number of currents will be the parameters that directly affect the stiffening performance. Due to the compactness of the mechanism, the overall size of the coil cannot be infinitely large. The more the diameter of the single wire coil increases, the higher the allowed current value. but at the same time, because of the increase in the diameter of the wire, the number of turns of the coil decreases, resulting in a decrease in the maximum negative stiffness peak.

Soft magnet material with relative permeability of $\mu_r = 1 \times 10^6$ is selected to construct the stator cores and mover armatures. The pole surface area of the stator cores is set as 10×10 mm^2. By considering the requirements of high energy efficiency, large achievable stroke, high compactness, and manufacturability, and are determined as 197 *mm*, 12 *mm*. The remaining parameters are listed in Table 1.

B. Analysis by finite element simulation

First, the electromagnetic force-displacement relationship to the armature is simulated by formulating the stator displacement. This physical model with mesh division is shown in Fig. 7(a). Fig. 7(b) shows the flux distribution and flux density modes on both sides when the armature is positioned with the intermediate equilibrium position. To further investigate the negative stiffness generated by the electromagnetic drive, the force-displacement curve and the stiffness-displacement curve during the change of current *I* from 1A to 10A with the number of turns *N* set to 140, the results are shown in Fig. 8(a) and Fig. 8(d), which are plotted based on the simulation results. From the simulation results, it can be seen that as the current increases, the negative stiffness formation generated by the NESTA increases. This negative stiffness increases as it moves away from the position. When the current is at 10A, the negative stiffness generated by the electromagnetic actuator can reach $10^5 N/m$.

In addition, it is worth that the negative stiffness of the magnetic field changes more linearly with distance from 0.5 mm to -0.5 mm away from the equilibrium position, so it is reasonable to design the stroke of the flexible mechanism in this range.

Finally, the finite element analysis of the electromagnetic-mechanical multi-physical field is developed, as shown in

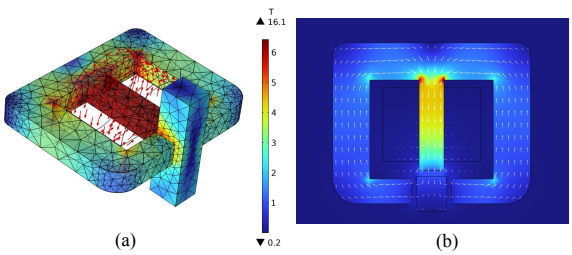

(a) (b)

Fig. 7. Finite element modeling of the electromagnetic negative stiffness (a) grid division (b) distribution of electromagnetic negative stiffness

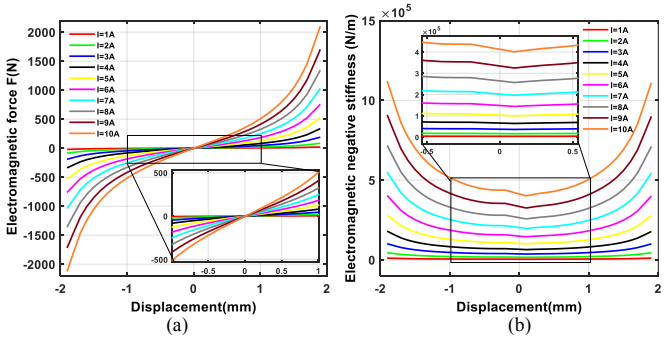

Fig. 8. The finite element simulation results of electromagnetic negative stiffness (a) curve of electromagnetic force associated with displacement (b) Curve of electromagnetic negative stiffness associated with displacement

Fig. 9. The stiffness distribution of the variable stiffness mechanism within the 2*mm* air gap design stroke and the variation with the excitation current were calculated by simulation which are shown in Fig. 10.

When the current is 0, the calculated stiffness is 1.438×10^5 and the simulated stiffness is 1.585×10^5, with an error of 9.27%. As the current increases from 0-10A, the stiffness obtained from the mathematical model decreases from 1.438×10^5 to 1.054×10^5, a decrease of 38%. The simulation model decreases from 1.585×10^5 to 1.095×10^5, a decrease of 30.9%, with a difference of 7.1%, as shown in Fig. 11. From the simulation results, the designed

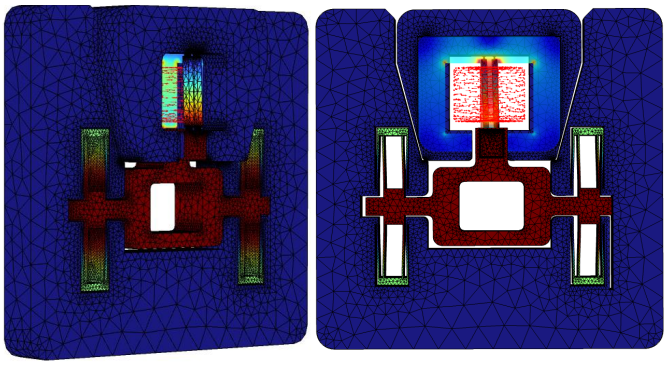

Fig. 9. Multi-physics field coupling simulation analysis of variable stiffness mechanism

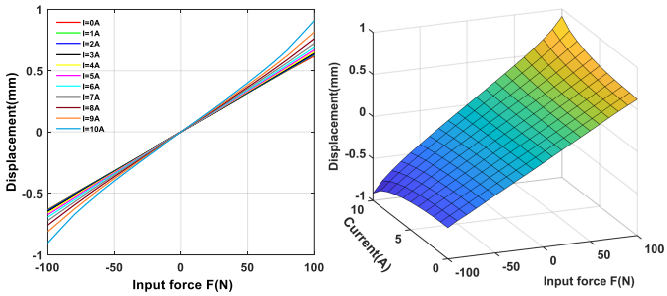

Fig. 10. Curve of stiffness with armature position under different excitation currents

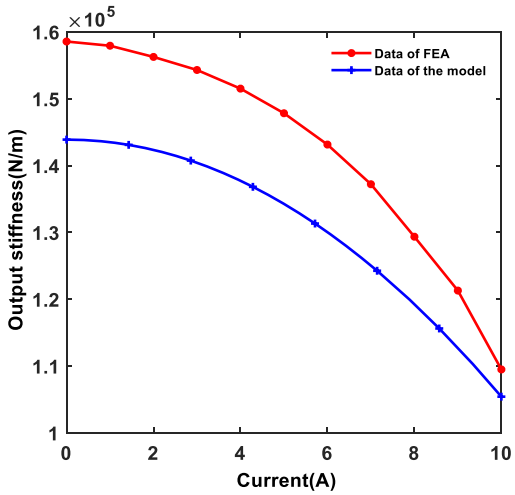

Fig. 11. Comparison of model and simulation stiffness adjustment

variable stiffness mechanism offers a wide adjustment range of stiffness, but the linearity of its adjustment stiffness is limited by air gap and stroke. Therefore, a reasonable air gap and working stroke should be fully considered in practical applications to the stable application of the variable stiffness mechanism.

V. CONCLUSIONS

In this paper, a variable stiffness mechanism is reported, which enables the adjustment of stiffness by adjusting the electromagnetic excitation current. It provided stiffness coupling through the parallel connection between a novel normal-stress electromagnetic stiffness tunable actuator and the flexible guide assembly. In order to more accurate evaluation the stiffness adjustment capability of the variable stiffness mechanism, a stiffness model of the electromagnetic and flexible components was also developed. In addition, finite element simulation analysis was performed to obtain the adjustment curve of electromagnetic negative stiffness. Moreover, the nonlinear problem of stiffness adjustment was evaluated by multi-physics coupling simulation to analyze the relationship between stiffness and displacement variation of variable stiffness mechanism, which provides the theoretical and numerical basis for the application of the NESTA based variable stiffness mechanism.

ACKNOWLEDGMENT

This work was supported in part by the Major Basic Research Program of the Natural Science Foundation of Shandong Province under Grant ZR2019ZD08, in part by the National Natural Science Foundation of China under Grant 51775319, and in part by the Science and Technology Project of Shenzhen City under Grant JCYJ20180305164242690.

REFERENCES

[1] Y. Chen, "Nanofabrication by electron beam lithography and its applications: A review.". Microelectronic Engineering, vol. 135, pp. 57-72, 2015,

[2] Y. Tang, A. Sandoughsaz, K. J. Owen, et al, "Ultra deep reactive ion etching of high aspect-ratio and thick silicon using a ramped-parameter process.". Journal of Microelectromechanical Systems, vol. 27, no.4, pp. 686-697, 2018.

[3] K. Cooper, "Scalable nanomanufacturing—A review". Micromachines, vol. 8, no. 1, pp. 20, 2017.

[4] M. Loganathan, A. Al-Ogaidi, D. A, Bristow. "Design and control of a dual-probe atomic force microscope". IEEE/ASME Transactions on Mechatronics, vol. 23, no. 1, pp. 424-433, 2017.

[5] H. Kim, D. E. Lim, Lee S, "Deep learning-based dynamic scheduling for semiconductor manufacturing with high uncertainty of automated material handling system capability". IEEE Transactions on Semiconductor Manufacturing, vol. 33, no. 1, pp. 13-22, 2020.

[6] D. Zhao, Z. Zhu, P. Huang, et al. "Development of a piezoelectrically actuated dual-stage fast tool servo". Mechanical Systems and Signal Processing, vol. 144, pp.106873, 2020.

[7] Y. Wei, Q. Xu. "Design and testing of a new force-sensing cell microinjector based on small-stiffness compliant mechanism". IEEE/ASME Transactions on Mechatronics, vol.26, no.2, pp. 818-829, 2020.

[8] J. Qian, P. Yan, P. Liu. "Position/force modeling and analysis of a piezo-driven compliant micro-gripper considering the dynamic impacts of gripping objects". Smart Materials and Structures, vol. 30, no. 7, p. 075036, 2021.

[9] F. Niu, Z. Liu, H. Gao, et al. "An enhanced cascade constant-force system based on an improved low-stiffness mechanism". Mechanism and Machine Theory, vol. 167, p.104544, 2022.

[10] Y. Tian, C. Zhou, F. Wang, et al. "Design of a flexure-based mechanism possessing low stiffness and constant force". Review of Scientific Instruments, vol. 90, no. 10, p. 105005, 2019.

[11] Z. Li, W. Chen, J. Zhang, et al. "A novel cable-driven antagonistic joint designed with variable stiffness mechanisms". Mechanism and Machine Theory, vol.171 p. 104716, 2022.

[12] Y. Shao, W. Zhang, X. Ding. "Configuration synthesis of variable stiffness mechanisms based on guide-bar mechanisms with length-adjustable links". Mechanism and Machine Theory, vol. 156, p.104153, 2021.

[13] X. Li, H. Zhu, W. Lin, et al. "Structure-Controlled Variable Stiffness Robotic Joint Based on Multiple Rotary Flexure Hinges". IEEE Transactions on Industrial Electronics, vol.68, no. 12, pp. 12452-12461, 2020.

[14] Q. Zhang, P. Yan, H. Wang. "A curved-beam based quasi-constant force mechanism supporting large range and force-sensitive robotic manipulation". Mechanism and Machine Theory, vol. 172, p. 104799, 2022.

[15] Y. S. Wu, C. C. Lan. "Linear variable-stiffness mechanisms based on preloaded curved beams". Journal of Mechanical Design, vol. 136, no. 12, 2014.

[16] H. Zhao, D. Han, L. Zhang, et al. "Design of a stiffness-adjustable compliant linear-motion mechanism". Precision Engineering, vol. 48, pp. 305-314, 2017.

[17] S. Ito, S. Troppmair, B. Lindner, et al. "Long-range fast nanopositioner using nonlinearities of hybrid reluctance actuator for energy efficiency". IEEE Transactions on Industrial Electronics, vol.66, no. 4, pp. 3051-3059, 2018.

[18] S. Yuan, Y. Sun, M. Wang, et al. "Tunable negative stiffness spring using maxwell normal stress". International Journal of Mechanical Sciences, vol. 193, pp. 106127, 2021.

[19] G. Stadler, E. Csencsics, S. Ito, et al. "High Precision Hybrid Reluctance Actuator with Integrated Orientation Independent Zero Power Gravity Compensation". IEEE Transactions on Industrial Electronics, vol. 69, no. 12, pp. 13296-13304, 2021.

[20] H. Pu, S. Yuan, Y. Peng, et al. "Multi-layer electromagnetic spring with tunable negative stiffness for semi-active vibration isolation". Mechanical Systems and Signal Processing, vol. 121, pp. 942-960, 2019.

[21] J. Qian, P. Yan. "Design and analysis of a compliant micro-gripper with LBL type displacement amplifier". 2019 IEEE International Conference on Manipulation, Manufacturing and Measurement on the Nanoscale (3M-NANO). IEEE, 2019.